Discrimination between emboli and artifacts for outpatient transcranial Doppler ultrasound data

Blaise Kévin Guépié, Bruno Sciolla, Fabien Millioz, Marilys Almar, Philippe Delachartre

Noname manuscript No.
(will be inserted by the editor)

Discrimination between emboli and artifacts for outpatient transcranial Doppler ultrasound data

Blaise Kévin Guépié · Bruno Sciolla · Fabien Millioz · Marilys Almar · Philippe Delachartre

Received: date / Accepted: date

Abstract This paper addresses the detection of emboli in transcranial Doppler ultrasound data acquired from an original portable device. The challenge is the removal of several artifacts (motion and voice) intrinsically related to long-duration (up to 1h 40mn per patient) outpatient signals monitoring from this device, as well as high intensities due to the stochastic nature of blood flow. This paper proposes an adapted removal procedure. This firstly consists of reducing the background noise and detecting the blood flow in the time-frequency domain using a likelihood method for contour detection. Then, an hierarchical extraction of features from magnitude and bounding-boxes is achieved for the discrimination of emboli and artifacts. After processing of the long-duration outpatient signals, the number of artifacts predicted as emboli is considerably reduced (by 92% for some parameter values) between the first and the last step of our algorithm.

Keywords Emboli detection · transcranial Doppler · ultrasound · time-frequency approach · likelihood · spectral kurtosis · artifacts rejection.

B. Guépié
Univ Lyon, INSA-Lyon, Universit Claude Bernard Lyon 1, UJM-Saint Etienne, CNRS, Inserm, CREATIS UMR 5220, U1206, F69621, LYON, France
E-mail: blaise-kevin.guepie@creatis.insa-lyon.fr

P. Delachartre
Univ Lyon, INSA-Lyon, Universit Claude Bernard Lyon 1, UJM-Saint Etienne, CNRS, Inserm, CREATIS UMR 5220, U1206, F69621, LYON, France
E-mail: philippe.delachartre@creatis.insa-lyon.fr

M. Almar
Atys Medical 17, Parc d'Arbora 69510 Soucieu en Jarrest - FRANCE E-mail: marilys.almar@atysmedical.com

1 Introduction

Accurate detection of cerebral emboli is an important medical challenge, as they are related to the risk of strokes [28], and provide considerable information on cerebral embolization risks during carotid artery stent placement procedures [8]. Reliable detection of emboli is therefore an essential step in the making of appropriate patient-management decisions.

In this paper, transcranial Doppler ultrasound, a cheap, portable and non-invasive technique, is applied to the middle cerebral artery to potentially detect emboli [22]. Emboli are defined as high-intensity transient signals (HITS). Several methods have been proposed to reliably identify them using transcranial Doppler signals, with most of them relying on a signal processing approach. The underlying idea of these methods is to define a statistical parameter for detecting HITS, which are considered as emboli. In [16] and [10], emboli detectors using a time series model or cardiac cycle energy model were proposed. Other authors have used linear projections (such as short-time or fractional Fourier transforms, or wavelet transforms and their derivatives) as detection statistics [9], or as features for event classification [2, 7, 15, 25, 14, 12, 13]. In other words, they try to classify events into emboli and artifacts. In [26], authors use blood velocity information into the dual-gated system for suppressing artifacts.

In this paper, all the HITS which are not emboli are considered as artifacts. Thus, artifacts group contains motion artifacts, voice artifacts, electrical artifacts, and high intensities due to the stochastic nature of the blood flow. The major above-mentioned methods addressed emboli detection using short-time signals to analyze immobilized patients; this implies that few artifacts are present in the considered signals. Because

emboli appear unpredictably, it is essential to perform monitoring over long time periods (several hours). One recent technological development that helps to realize this possibility is a miniaturized portable device with a robotized probe using a mono-gate system, the TCD-X device (Atys Medical, France), which allows monitoring outside of a hospital room, thereby releasing hospital resources. The outpatient monitoring leads to increase the number of artifacts particularly those from speaking and motion. The removal of artifacts is generally a serious problem in the biomedical signal domain, such as in electroencephalography (EEG) and functional near-infrared spectroscopy [27, 1] because artifacts can corrupt the integrity, and hence compromise the interpretation of monitoring signals.

The aim of this paper is to propose an approach that can reliably detect emboli on transcranial Doppler data derived from a portable device. The innovative part of this study is the procedure for removing artifacts. Following the previous papers of Biard et al. [3, 4], we deepen the detection of emboli by artifacts rejection using their shapes in the time-frequency or time-velocity domain (thanks to the Doppler effect), instead of the time domain, where the discrimination of emboli and artifacts appears difficult to achieve (see Figures 1a, 1b, 1c and 1d). The underlying concept is to use both the time and the velocity information to improve the detection results. For example, superimposed signals of a motion artifact and an embolus can be better separated in the time-frequency domain, because the motion is composed of lower frequencies than the embolus [4, 26]. The proposed method is able to detect emboli from long time-course outpatient acquired signals. It covers both the detection of HITS (or potential emboli signal extraction) and the classification of extracted signals (or artifacts removal). Our procedure is composed of three main steps. Firstly, the maximum instantaneous velocity of the blood flow is determined; it gives the time-frequency area containing the blood flow. This determination is achieved using a robust segmentation approach based on the likelihood method. Then, a method based on spectral kurtosis is implemented to estimate the average magnitude onto the previous detected blood flow area, and determine the HITS threshold. Secondly, relevant parameters for removing artifacts from detected HITS are investigated. Finally, the remaining HITS are projected onto a feature space for the classification of emboli and artifacts using support vector machines (SVM).

This paper is organized as follows. Section 2 is devoted to the problem statement. Section 3 describes our proposed approach, including the detection of HITS, processing, and classification tools. Section 4 demonstrates and discusses the emboli detection performance on real data from patients. Conclusions on the work are then made in Section 5.

2 Problem statement

After analyzing the literature [3, 26, 2] and our database of outpatient transcranial Doppler monitoring, the difference of emboli and artifacts are hierarchically given by the following line:

1. emboli frequency components are in the range of those of the blood flow;
2. emboli have intense magnitude value;
3. emboli are unidirectional or non-symmetrical;
4. emboli appear at most two times in a period of 0.5 second;
5. emboli have large surface of bounding-boxes and large number of connected intense values in the time-frequency representation;
6. emboli ratio of the frequency spreading over the duration is high.

Figures 1a and 1b show the quadrature transcranial Doppler signals of an embolus and an artifact respectively, while Figures 1c and 1d display the spectrograms of these events. As previously mentioned in [2], these gures show that using both the time and velocity information, rather than using only the time information (audio samples), gives better results in the separation of the symmetrical artifacts and emboli.

Spectrograms show two image parts, the first of which is composed of background noise. It is present in both the positive and negative velocity (outside area Ω_1 in Figures 1c and 1d). The second part is the blood flow, which is a non-stationary signal and is present in the positive velocity (see Ω_1 in Figures 1c and 1d). An embolus is represented by HITS visible in only the second part (the blood flow), while an artifact may be visible outside of the blood flow area, in the time-velocity image.

The problem of emboli detection can therefore be split into two main parts. The first part, called the HITS detection, consists of separating HITS from the blood flow. It can be mathematically formulated according to the following lines. The model of the Doppler signal of blood flow (without HITS) in the time-velocity domain is

$$s(n,k) = \begin{cases} \xi(n,k) \text{ if } (n,k) \in \Omega_1 \\ \epsilon(n,k) \text{ if } (n,k) \in \Omega_0 \end{cases}, \quad (1)$$

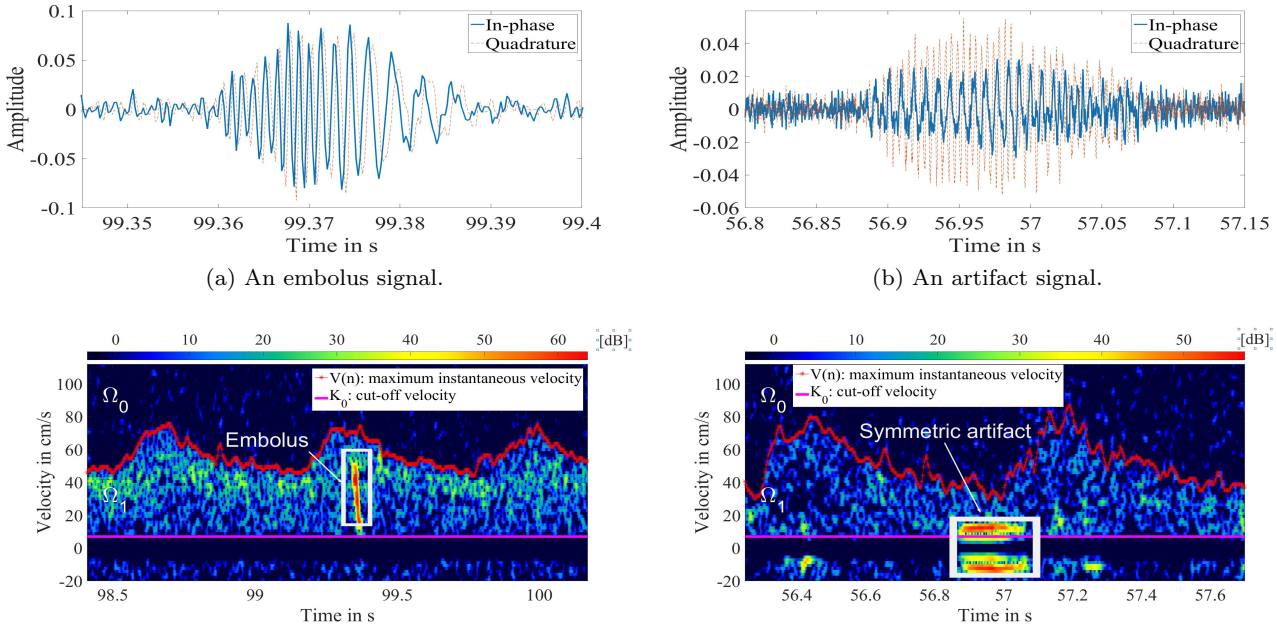

(a) An embolus signal.

(b) An artifact signal.

(c) Spectrogram of the embolus in Figure 1a.

(d) Spectrogram of the artifact in Figure 1b.

Fig. 1: Example of HITS representations.

and the model of the Doppler signal of blood flow in the time-velocity domain when HITS arise is

$$s(n,k) = \begin{cases} \gamma(n,k) + \xi(n,k) & \text{if } (n,k) \in \Omega_1 \\ \epsilon(n,k) & \text{if } (n,k) \in \Omega_0 \end{cases}, \quad (2)$$

where n is the time index, k is the velocity index, $s(n,k)$ is the short-time Fourier transform (STFT), $\{\epsilon(n,k)\}$ is a random variable sequence of unknown law, $\{\xi(n,k)\}$ is assumed to be a sequence of independent identically distributed (i.i.d) circular complex Gaussian variables with zero mean and unknown variance σ^2, and $\gamma(n,k)$ is the STFT of HITS. Sets Ω_1 and Ω_0 are respectively given by

$$\begin{aligned} \Omega_1 &= \{(n,k)\,|\,1 \le n \le N_e,\ K_0 \le k \le V(n)\}, \\ \Omega_0 &= \{(n,k)\,|\,1 \le n \le N_e,\ V(n) < k \le K_e\}, \end{aligned} \quad (3)$$

where K_0 is the cut-off frequency index of a high-pass filter applied to the data to remove the DC component, N_e is the index of rows related to the considered signal duration, K_e is the columns index for the maximum detectable velocity (related to the pulse repetition frequency), and V is the unknown mapping characterizing the maximum instantaneous velocity of the blood flow. Detection of HITS is equivalent to deciding if $\gamma(n,k) = 0$ or not, i.e, to deciding one the true model between (1) and (2).

The second main sub-problem consists of classifying the detected HITS into artifacts and emboli groups.

3 Proposed method

3.1 Procedure description

As outlined in Figure 2, the major steps of our proposed method are as follows.

- Detection of HITS. This is achieved through three sequential steps:
  1. Segmentation of the time-frequency representation into two areas by using the likelihood method. The First area is the blood flow part called Ω_1 and the second one is outside area Ω_1 (i.e., the background noise part). This is equivalent to the estimation of the maximum instantaneous velocity of the blood flow.
  2. Estimation of the average blood flow magnitude from the part Ω_1 despite the presence of emboli and artifacts using the spectral kurtosis approach.
  3. Detection of HITS by applying the Neyman-Pearson method on the average blood flow magnitude.
- Analysis of detected HITS and removal of several artifacts: some characteristics such as the symmetry, bounding-box surface, and the number of intense magnitude points, are evaluated for HITS and used to eliminate artifacts.
- Extraction of features and classification of the remaining HITS into emboli and artifacts groups.

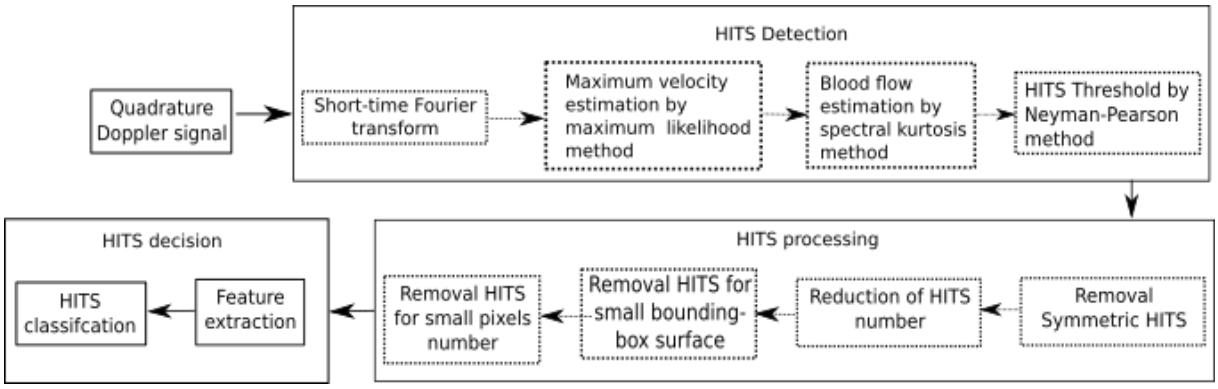

Fig. 2: The framework of the emboli detection process.

3.2 Detection of HITS

3.2.1 Estimation of the maximum instantaneous velocity

This step is essential to achieve a correct detection of HITS in 3.2.2. Let us define the time-velocity image by Ω. Our contour detection method is based on the popular likelihood approach [23], which outperforms several approaches based on the maximization of two density function distances [24]. It is briefly explained as follows. The separation of Ω into two separate areas Ω_0 and Ω_1 such as $\Omega = \Omega_0 \bigcup \Omega_1$ can be done by testing two statistical hypotheses. Let us define V as

$$V : \{1, \cdots, N_e\} \longrightarrow \{K_0, \cdots, K_e\}$$

such as the set $\mathcal{C} = \{(n, V(n)), n \in \{1, \cdots, N_e\}\}$ is the boundary between Ω_0 and Ω_1. Let us assume that $X_S(n,k)$ is the sequence of independent random variables generating pixel values $S(n,k)$ where $S(n,k) = |s(n,k)|^2$ and $|\cdot|$ means the modulus . The two statistical hypotheses to test are

$$\begin{aligned} \mathcal{H}_0 &= \{X_S(n,k) \sim \mathcal{P}_0, \forall (n,k) \in \Omega_0 \bigcup \Omega_1\} \\ &\quad \text{vs} \\ \mathcal{H}_1 &= \begin{Bmatrix} X_S(n,k) \sim \mathcal{P}_1, \forall (n,k) \in \Omega_1 \\ X_S(n,k) \sim \mathcal{P}_0, \forall (n,k) \in \Omega_0 \end{Bmatrix} \end{aligned}, \tag{4}$$

where $\mathcal{P}_l$ for $l \in \{0,1\}$ are two different cumulative distribution functions. Hypothesis $\mathcal{H}_0$ supposes that all pixels derive from a common law $\mathcal{P}_0$ and $\mathcal{H}_1$ supposes that pixels of area Ω_0 and Ω_1 derive from two distinct laws $\mathcal{P}_0$ and $\mathcal{P}_1$. The log-likelihood ratio LL of this statistical test depends on the curve V, and is defined by

$$LL(V) = \ln \left(\frac{\prod\limits_{(n,k)\in\Omega_1} f_1(S(n,k)) \prod\limits_{(n,k)\in\Omega_0} f_0(S(n,k))}{\prod\limits_{(n,k)\in\Omega_0 \bigcup \Omega_1} f_0(S(n,k))} \right), \tag{5}$$

where f_l is the probability density function (pdf) of $\mathcal{P}_l$ for $l \in \{0,1\}$. From (1) and (2), no assumption is made about the background noise probability law $\mathcal{P}_0$. Thus, our approach is non-parametric. The pdf is then computed using a priori Parzen estimates [21].

The contour detection can be performed by initializing the boundary $\mathcal{C}$, and maximizing LL for all the possible values of the boundary. In practice, the contour is built at each period corresponding to a time-sample of the time-velocity image. Then, a regularization term inspired by [6] is added to LL before the maximization:

$$RT(V) = \alpha \sqrt{1 + [V(n-1) - V(n)]^2},$$

where $V(n-1)$ is the previous determined ordinate belonging to the maximum instantaneous velocity, $V(n)$ is the tested current ordinate, and α is a tuning parameter. The goal of this term is to avoid likely outliers. In summary, our boundary determination method is recursive and given by

$$\mathcal{C} \left\{ \left(n, \hat{V}(n) \right)_{N_0 \le n \le N_e} | \, \hat{V} = \arg\max_V \left[LL(V) - RT(V) \right] \right\}, \tag{6}$$

where N_0 is the number of pixels used for the algorithm initialization. The curve smoothing is achieved using a moving average filter.

The estimation of the maximum instantaneous velocity delimits the blood flow part Ω_1. Then, the next paragraph is dedicated to the determination of the average blood flow magnitude from this part Ω_1.

3.2.2 Blood flow magnitude estimation

Emboli are defined as HITS, and detection of them is difficult because it requires knowledge of the blood flow magnitude, i.e, the blood flow magnitude in absence of HITS. The main difficulty is to know whether the considered signal (or a part) contains HITS. To avoid this difficulty, a spectral kurtosis approach [18] is proposed. The spectral kurtosis approach is used on the selected part of the time-velocity image which is located between the index K_0 and the maximum instantaneous velocity.

HITS are of short duration with respect to the acquired Doppler signal. From (1) and (2), this implies that $\gamma(n,k)=0$ for almost all values of (n,k). Thus, as is mentioned in [18], for the smallest values of $|s(n,k)|$, the distribution of $s(n,k)$ is close to that of the circular complex Gaussian variable $\xi(n,k)$.

Under these conditions, the spectral kurtosis approach can separate HITS from the blood flow magnitude. Let us briefly present the spectral kurtosis approach. When an energy detector is used to detect HITS, thresholding of the energy means thresholding of the spectrogram. Removing points greater than a threshold h gives a truncated complex Gaussian variable Z_h depending on σ and h [18]. The spectral kurtosis $SK_{\sigma,h}$ of Z_h is defined by

$$SK_{\sigma,h}=\mathbb{E}(|Z_h|^4)/\mathbb{E}^2(|Z_h|^2)-2, \tag{7}$$

where $\mathbb{E}$ means the expectation. It follows that

$$SK_{\sigma,h}=\frac{\left(\exp\left\{(\frac{h}{\sigma})^2\right\}-1\right)\left(2(\frac{h}{\sigma})^2-(\frac{h}{\sigma})^4\right)-2(\frac{h}{\sigma})^4}{\left(\exp\left\{(\frac{h}{\sigma})^2\right\}-1-(\frac{h}{\sigma})^2\right)^2}. \tag{8}$$

From (8), it is clear that the spectral kurtosis depends only on the normalized threshold $h_n=h/\sigma$ and that it is an invertible function. There is therefore an unique $h_n(\kappa)$ such as

$$SK_{1,h_n(\kappa)}=\kappa. \tag{9}$$

The value of $h_n(\kappa)$ is approximated by numerically inverting (8). However, using (7), it is possible to find the non-normalized threshold $h(\kappa)$, such that the spectral kurtosis of the points smaller than $h(\kappa)$ is equal to the value κ:

$$SK_{\sigma,h(\kappa)}=\kappa. \tag{10}$$

The variance estimator $\hat{\sigma}^2_\kappa$ of blood flow in the STFT domain is then

$$\hat{\sigma}^2_\kappa=\left[h(\kappa)/h_n(\kappa)\right]^2. \tag{11}$$

This variance is also an estimation of the blood flow magnitude and depends on κ. Empirically, the value of $\hat{\sigma}^2_\kappa$ for $\kappa=(-0.3)$ has been found to be the most relevant in terms of bias and variance [18].

3.2.3 HITS threshold selection

HITS are detected as events whose spectrogram values $S(n,k)$ exceed a prescribed threshold. Because the STFT of blood flow is assumed to follow a Gaussian law, the spectrogram values $S(n,k)$ follow a chi-squared distribution. Thus, for a given value p_{fa} of false alarm probability (pfa), the optimal threshold h_1 is obtained from the uniformly most powerful test [19]:

$$h_1=\hat{\sigma}^2_{-0.3}\ln\left\{p_{fa}^{-1}\right\}. \tag{12}$$

Remark 1
After thresholding the time-velocity image, the sets of connected pixels whose values exceed h_1 together form one event.

3.3 Processing of HITS

In the remainder part of this paper, HITS are normalized by $\hat{\sigma}^2_{-0.3}$ in order to reduce their dependency to patients.

3.3.1 Removal of symmetrical HITS

As Remark 1, HITS are composed of connected pixels whose values exceed the threshold h_1 in the positive part of frequencies also called the flow (or forward flow) part. For all the HITS, the symmetrical location of connected pixels in the flow with respect to the abscissa, i.e., in the negative part of frequencies also called the back-flow (or reverse flow) is also considered. The average of pixel intensities or magnitudes in the flow and the back-flow are respectively called S_f and S_{bf}. Each high intensity event (an artifact or an embolus) corresponds to one value of S_f and S_{bf}. For artifacts, the distribution of the average magnitude ratio of the flow over the back-flow is bimodal. The first mode (small values of the ratio) is composed of symmetrical or bidirectional artifacts [3] such as the voice artifact in Figure 1d. The second mode (large values of the ratio) is composed of non-symmetrical artifacts such as electrical artifacts or high intensities due to the stochastic nature of the blood flow. In practice, the artifacts distribution is not known for a patient; although the distribution of HITS (emboli and artifacts) is known. The distribution of HITS is also bimodal because emboli belong to only the second

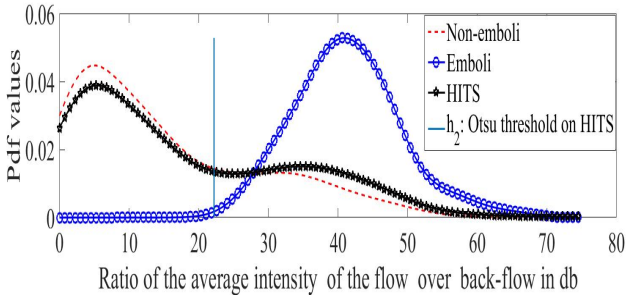

Fig. 3: Distribution of the average intensity ratio of the flow over the back-flow for patient No.1.

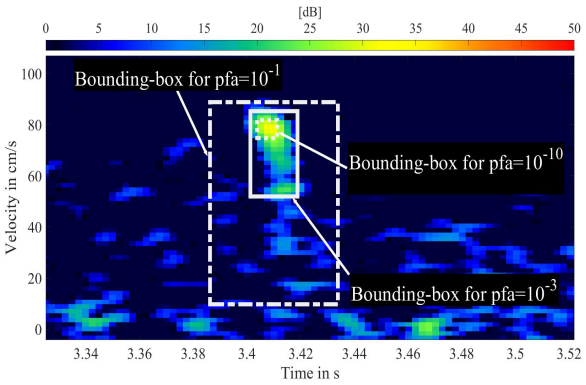

Fig. 4: Bounding-boxes for three values of pfa.

mode as it is shown in Figure 3. The plotted distributions are for the patient No.1. A statistical threshold h_2 for separating both the modes can be determined using the well-known Otsu algorithm [20]. Then, the rule for removing symmetrical HITS is then given by

- if $10\log 10(S_f/S_{bf}) \leq h_2$, HITS are considered as an artifact and removed;
- if $10\log 10(S_f/S_{bf}) > h_2$, HITS are kept and their group membership will be defined later.

3.3.2 Reduction of the number of HITS

After removing symmetrical artifacts, the remaining HITS are largely composed of blood flow magnitude (due to the stochastic nature of blood flow and the long duration of acquired signals) exceeding the prescribed threshold h_1. It is obvious that when an embolus arises, its signal is superimposed on the blood flow signal. Therefore, considering short time periods where the signal holds stationary, intense peaks are likely to be emboli, while the others are likely to be blood-flow outliers. After analyzing the database, we note that for the duration corresponding to half cardiac cycle, fewer than two emboli are present. Accordingly, only the two greatest HITS (w.r.t the magnitude) will be kept, and all the others will be removed at each considered window of a size approximating half cardiac cycle.

3.3.3 Removal of HITS for small bounding-box surfaces

The determination of the size of the bounding-box required to encompass HITS is not a trivial problem. To solve this problem, several pfa are empirically tested. Figure 4 shows bounding-boxes with respect to three pfa. For the first of these ($p_{fa} = 10^{-10}$), the threshold h_1 is high and the bounding-box is small w.r.t the considered embolus spectrogram. This results in only a small part of the visible embolus being detected. The bounding-box for $p_{fa} = 10^{-1}$ is obviously too large, while the bounding-box for $p_{fa} = 10^{-3}$ is visually the most appropriate for this embolus. This value is confirmed by the analysis of other HITS, and is therefore used throughout this paper. After determination of the bounding-box, HITS appearing at the same time (i.e., their bounding-box durations overlap) are concatenated. This avoids the confusing situation where two separated HITS are associated with the same detection time. In analyzing the pdf for the bounding-box surfaces of HITS, we noted that it is bimodal. Most of the emboli present with large values of bounding-box surfaces, whereas several artifacts (outliers of the blood flow magnitude) present with small values. This is why HITS with a bounding-box surface less than a determined threshold h_3 are removed. The separation threshold h_3 is also given by the Otsu algorithm.

3.3.4 Removal of HITS with a low pixel number

Several artifacts composed of aggregated high-magnitude blood flow have large bounding-box surfaces, and the previous technique fails to remove them. Nevertheless, counting the number of intense magnitudes in each bounding-box enables them to be identified and deleted. We also noted that the pdf of the intense magnitudes has a bimodal nature. Emboli generally have more intense magnitudes than the remaining artifacts. In this case, the Otsu method gives a threshold h_4 for removing these artifacts.

Remark 2 In order to avoid patient dependence on calculated values, the procedures described in the part 3.3.3 and 3.3.4 are normalized using the average of the maximum instantaneous velocity.

In brief, our proposed HITS processing procedure is given by algorithm 1.

Algorithm 1 HITS processing

1: Detect HITS (3.2.3).
2: Remove duplicate HITS.
3: Calculate for any HITS S_f and S_r, the respective average normalized magnitude in flow and back-flow (3.3.1).
4: Remove HITS if $10\log 10(S_f/S_{bf}) \leq h_2$ (3.3.1).
5: Keep only the two highest HITS (3.3.2).
6: Determine appropriate HITS bounding-boxes (3.3.3).
7: Concatenate HITS appearing at the same time (3.3.3).
8: Remove HITS if the bounding-box surface is less than h_3 (3.3.3).
9: Remove HITS if the number of intense magnitudes is fewer than h_4 (3.3.4).

3.4 HITS decision

3.4.1 Feature extraction

The analysis of several time-velocity images shows that most emboli are of short duration, with a spread of velocities. This implies that the ratio of height over width for the bounding-boxes is large, whereas for several artifacts, this ratio is small. Additionally, when the ratio of height over width for a detected embolus is small, its magnitude is traditionally higher than the other HITS. The two dimensional space formed by the magnitude and the ratio of height over width is then selected as a feature space. The projections of HITS can be separated in this space, and this will be performed in the next paragraph.

3.4.2 Weighting of the SVM for classification

In machine learning domain, several methods exist for separating data. For labeled data, the SVM can achieve excellent performance according to [5]. Traditionally, SVM have been used to separate two groups. The principle is to maximize the separation margin; the margin being the distance between the closest observations of the two groups. Consider a given training set $\{x_\ell, y_\ell\}_{1\leq\ell\leq N}$ with the observation $x_\ell \in \mathbb{R}^d$ and the class variable $y_\ell \in \{-1, 1\}$. Suppose that data are linearly separable, i.e, there exists a linear classifier(w, w_0) such as

$$\begin{cases} \langle w, x_\ell\rangle + w_0 \geq +1 \text{ if } y_\ell = +1 \\ \langle w, x_\ell\rangle + w_0 \leq -1 \text{ if } y_\ell = -1 \end{cases}, \tag{13}$$

where $\langle , \rangle$ is the dot product. The problem of finding the separator which maximizes the margin is equivalent to :

$$\begin{aligned} &\min_{w,w_0} \frac{1}{2}\langle w, w\rangle \\ &\text{constraint to } y_\ell(\langle w, x_\ell\rangle + w_0) \geq 1,\ 1 \leq \ell \leq N. \end{aligned} \tag{14}$$

Generally, data are not linearly separable. The trick is to project them onto a high-dimensional feature space using a non-linear map $\psi(\cdot)$, such that the projections are linearly separable. Therefore, slack variables $\mu_\ell \geq 0$ are introduced to solve the problem. The optimization problem becomes

$$\begin{aligned} &\min_{w,w_0,\mu\ell} \frac{1}{2}\langle w, w\rangle + C\sum_{\ell=1}^{N}\mu_\ell \\ &\text{such that } \begin{cases} y_\ell(\langle w, \psi(x_\ell)\rangle + w_0) > 1 - \mu_\ell \\ \mu_\ell \geq 0 \end{cases}, \end{aligned} \tag{15}$$

where C is a positive constant determining the SVM tolerance of the poorly separated observations. Passing by the dual form of (15), the calculation of projections $\psi(x)$, $\forall x$ is needless; only the computation of $\left\langle \psi(x^{'}), \psi(x) \right\rangle$, $\forall(x^{'}, x)$ is required [11]. Thanks to Mercers condition [17], the latter dot product, which often requires a lot of computational resources, is replaced by the calculation of a kernel $K(x^{'}, x)$. Traditionally, a Gaussian kernel is used.

When the ratio of observations number r between the positive ($y_\ell = 1$) and negative ($y_\ell = -1$) training groups is far from one, the SVM separator is biased, and it is close to the group containing most of the observations. This is why, authors in [11] use $C^+ = \frac{rC}{r+1}$ and $C^- = \frac{C}{r+1}$ for the positive and negative group respectively, instead of C. In order to render C^+ and C^- more flexible, and to then improve the detection performance on our database, we propose using $C^+ = \left(\frac{r}{r+1}\right)^\beta C$ and $C^- = \left(\frac{1}{r+1}\right)^\beta C$ instead of their previous definitions. The parameters β and C, and the Gaussian kernel width, are determined by a 10-fold cross validation procedure.

4 Experimental results and discussion

4.1 Data description

Our database is composed of outpatient acquired signals from twelve patients with a carotid stenosis. A carotid stenosis is a narrowing or blockage of the carotid arteries due to an accumulation of organic or mineral material. It is a dangerous illness, as some aggregated materials may break off, move to cerebral arteries, and block them, thus causing a stroke. In the monitoring analyzed in this study, the following TCDX parameters were used. The pulse repetition frequency (PRF) was between 4 and 5 kHz. The emitted waves had a central frequency equal to 1.5 MHz and lasted 10 s. The

received signals were demodulated at the emitted signal frequency by a quadrature demodulation leading to two channel signals. The labeling of emboli is achieved by two experts belonging to the Atys Medical company. The first expert detected emboli from the acquired patient data, and the second expert validated or not the emboli detected by the first expert. Table 1 shows the number of detected emboli by this labeling procedure.

4.2 Comparison of emboli detection performance

In this section, we compare the performance of our proposed emboli detector with that of the Naive Bayes (N-Bayes) investigated in [13] and the MI-HDMR introduced in [12]. These latter algorithms have recently been described, and they outperform several other short-time HITS classifiers. Therefore, it is of interest to know their performance on long-duration outpatient data acquired from the portable Doppler device.

The MI-HDMR and N-Bayes algorithms parameters for all patients were as follows. Training used 192 signals (blood flow, artifacts and emboli) of size 1 s from five patients. For testing, patient signals were split into windows of 1 s, with 50% overlap. The mother wavelet was the eighth-order Daubechies wavelet and the maximum used scale was eight. The training step used signals originating from five different patients.

For all the patients, the remaining parameters used for our algorithm were as follows. The STFT used 128 points, and the Blackman window had a 91% overlap. The tuning parameter α, the number of initial pixels N_0, and the cut-off frequency for determining the maximum instantaneous velocity were 0.5, 100 pixels, and 150 Hz respectively. For HITS detection, the sliding window in the time-velocity domain was 1 s, with a 50% overlap. The appropriate pfa for the HITS bounding-box was fixed to $p_{fa} = 10^{-3}$ before calculating h_3 and h_4.

Thresholds h_2, h_3 and h_4 for removal of artifacts, were automatically evaluated through the Otsu method. Table 2 shows example values with $p_{fa} = 10^{-6}$.

The exact number of artifacts for the MI-HDMR and the N-Bayes, and their emboli detection probabilities are known. Nevertheless, it is not easy to calibrate our method to have exactly the same number of artifacts or the same emboli detection probability than the MI-HDMR and N-Bayes methods. In order to make a comparison, we proceeded as follows. An emboli detection is achieved either by the N-Bayes or by the MI-HDMR method. For our method, a list of pfa values is selected and detection is achieved for each pfa value into the list. This gives an invertible performance curve

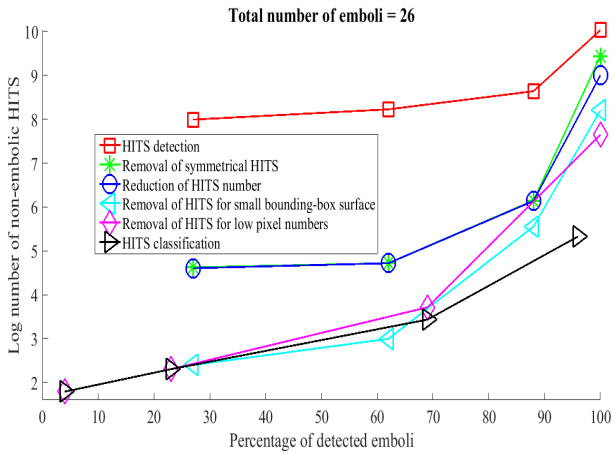

Fig. 5: Algorithm performances evolution for patient No.4

for our method showing the number of artifacts as a function of the emboli detection probability (see for example, the HITS detection and classification curves in Figure 5). Then, our method can give the number of artifacts related to the same value of the emboli detection probability given either by the N-Bayes or by the MI-HDMR method. The comparison of the number of artifacts between the N-Bayes and our method for all patients is shown in Table 3., and the comparison between the MI-HDMR and our method is shown in Table 4

From the previous pfa list, Figure 5 shows an example of curves at each step of our algorithm. Considering all patients, between the first step (HITS detection) and last step (HITS classification) of our algorithm, the artifacts predicted as emboli were reduced by 92%. The reduction of artifacts for our method comparatively to N-Bayes and MI-HDMR are respectively 35% and 82%.

4.3 Discussion

Thresholds h_1 to h_4 are automatically calculated by our algorithm, with h_1 taking several values for the same patient, depending on the current sliding window. It is therefore adaptive to any increase or decrease in the signal amplitude during monitoring. The variation of thresholds h_2 to h_4 in Table 2 are due to the fact that the acquired patient signals are very different. In old patients, bone calcification is greater, and the received flow signal is lower than in younger patients. The values of h_3 and h_4 in dB are negative because of the normalization explained in Remark 2.

Because our database contains outpatient data signals, several artifacts (motion and voice) are present

Table 1: Database description.

Patients	*No.*1	*No.*2	*No.*3	*No.*4	*No.*5	*No.*6	*No.*7	*No.*8	*No.*9	*No.*10	*No.*11	*No.*12
Signals duration (s)	323	480	157	1620	3921	5995	111	4541	3377	3571	601	300
Number of emboli	65	16	36	26	5	18	28	8	3	23	43	29

Table 2: Thresholds for artifact removal procedure.

Patients	*No.*1	*No.*2	*No.*3	*No.*4	*No.*5	*No.*6	*No.*7	*No.*8	*No.*9	*No.*10	*No.*11	*No.*12
h_2 in dB	25	34	41	43	46	25	21	24	27	32	31	31
h_3 in dB	-8	-8.1	-6.8	-6.2	-7.7	-9.7	-8.12	-10.35	-4.32	-18.10	-1.78	-3.6
h_4 in dB	-19.6	-25.5	-26.6	-25.2	-27.7	-28.7	-21.13	-17.96	-10.90	-24.29	-11.67	-16.47

Table 3: Comparative detection performance of N-Bayes and our method.

		Patient No.											
	Method	1	2	3	4	5	6	7	8	9	10	11	12
% of emboli detected	N-Bayes	44.61	62.5	66.67	61.53	100	50	60.71	87.5	100	91.3	86.04	44.82
Number of artifacts per min	N-Bayes	25.3	20.8	35.2	28.8	9.1	41.7	18.4	26.1	24.6	32.1	60.9	22
	Ours: 1^{st} step	55	16.4	37.5	138.4	20	37.3	203.82	147.29	258.46	542.52	275.89	225.37
	Ours: 6^{th} step	1.76	0.11	1.15	1.02	0.08	0.08	0	4.2	103.44	16.7	43.22	22.96

Table 4: Comparative detection performance of MI-HDMR and our method.

		Patient No.											
	Method	1	2	3	4	5	6	7	8	9	10	11	12
% of emboli detected	MI-HDMR	18.5	31.2	55.6	73.1	60	33.3	39.3	62.5	33.3	87	48.8	6.9
Number of artifacts per min	MI-HDMR	17.46	23.88	19.87	31.37	26.17	17.45	17.29	37.59	16	39.28	21.76	8
	Ours: 1^{st} step	22.75	8.2	31.2	168.8	12	24.9	131.9	105.4	86.2	473.9	113.4	13.9
	Ours: 6^{th} step	0.74	0.06	0.64	2.07	0.05	0.06	0	3	10.19	16.85	13.29	10.2

most of the time. For example, patient No.4 talks very long time during the monitoring (75% of the monitoring duration). This causes very high number of artifacts than several others monitored patients. It therefore follows that when an embolus occurs, its signal is close to some artifact signals.

Tables 3 and 4 show the performance of our method, and those of two previous methods for emboli detection: the N-Bayes investigated in [13] and the MI-HDMR introduced in [12]. The major difference of our method than the N-Bayes and the MI-HDMR is the using of features from time-frequency representation for artifacts rejection. Indeed, the MI-HDMR algorithm and the N-Bayes aforementioned use the EBR (embolus to blood ratio) parameter and time and frequency features separately for deleting artifacts. Nevertheless, these time or frequency features are not easy to estimate properly because of the proximity of artifacts (voice and motion for example) and emboli most of the time. Our algorithm enables the separation of emboli from most of the voice and motion artifacts using a two-dimensional space: the time-frequency representation. In fact, these artifacts are of low frequency than emboli. Moreover, although emboli and artifacts signals are close or superimposed, they can still be separated by time-frequency features based on events shape such as bounding-box surface, ratio of frequency spreading over the duration.

With consideration of all the patients, a comparison of the first step of our algorithm with N-Bayes and MI-HDMR shows that without an appropriate artifacts removal step, the N-bayes and the MI-HDMR perform better on average (respectively 83% and 56% fewer artifacts) than our algorithm. Nevertheless, after appropriate processing, our algorithm performs better on average than the N-Bayes and the MI-HDMR (respectively 35% and 82% fewer artifacts).This demonstrates the importance of our artifacts removal procedure for outpatient data monitoring. Additionally, all the parameter values of our algorithm are automatically estimated. This makes our algorithm more robust to patient-specific differences.

For the same number of detected emboli, the artifacts wrongly predicted as emboli from patients are different. This can be explained by the difference in EBR, and the number or type of artifacts present before detection. Figure 5 shows that our algorithm steps are adapted to removal of artifacts. From step one to four, the number of artifacts, decreases substantially while the number of detected emboli is almost the same. Step four is sometimes above step five, meaning that no order can rationally be given between artifacts removal w.r.t the bounding-box surfaces, and artifacts removal w.r.t the number of intense magnitudes belonging to bounding-boxes. Indeed, both these steps are complementary.

In practice, four our method, it is not yet possible to fix the tolerated number of artifacts/min before detection. One way to overcome this limitation would be to propose a list of pfa values, and to take the HITS detection result relative to the pfa value closest to, but below, this tolerated number of artifacts/min.

5 Conclusion

This paper proposes an automatic algorithm (i.e, not operator-dependent) for emboli detection adapted to the long duration of outpatient data monitoring from a new miniaturized and portable transcranial Doppler ultrasound device. The originality is the procedure for removing artifacts, which generally come from the patients voice and motion. Our detection is achieved in the time-frequency domain. The main steps can be described as follows. Firstly, the background noise is reduced, then the blood flow magnitude is estimated and high-intensity transient signals (HITS) are detected. Finally, artifacts are suppressed from detected HITS by a combination of magnitude and duration and frequency and time-frequency shape (bounding-box) parameters. Considering the long duration of outpatient signal monitoring, the percentage of artifacts predicted as emboli was considerably reduced (by 92% for some detection parameters) between the first and the last step of our algorithm. This means that our procedure is adapted to this kind of signal.

Future work should test this algorithm on a larger set of data, and classify detected emboli into solid and gaseous groups to satisfy a medical requirement.

Acknowledgements This work was funded by the ANR-13-LAB3-0006-01 LabCom AtysCrea and was supported by the LABEX CELYA (ANR-10-LABX-0060) and PRIMES (ANR-11-LABX-0063) of Université de Lyon, within the program "Investissements d'Avenir" (ANR-11-IDEX-0007) operated by the French National Research Agency (ANR).

References

1. Abbaspour S, Fallah A (2014) Removing ecg artifact from the surface emg signal using adaptive subtraction technique. Journal of Biomedical Physics & Engineering 4(1):33
2. Aydin N, Marvasti F, Markus H (2004) Embolic doppler ultrasound signal detection using discrete wavelet transform. Information Technology in Biomedicine, IEEE Transactions on 8(2):182–190
3. Biard M, Kouamé D, Girault JM, Patat F (2003) Discrimination between emboli and artifacts during transcranial doppler. In: Proceedings of the World Congress on Ultrasonics, Société française d'acoustique, WCU 2003, pp 1101–1104
4. Biard M, Kouamé D, Girault J, Souchon G, Guibert B (2004) Casc : caractrisation du sang circulant. ITBM-RBM 25(5):283–288
5. Caruana R, Niculescu-Mizil A (2006) An empirical comparison of supervised learning algorithms. In: Proceedings of the 23rd International Conference on Machine Learning, ACM, New York, NY, USA, ICML '06, pp 161–168
6. Chan T, Vese L (2001) Active contours without edges. Image Processing, IEEE Transactions on 10(2):266–277
7. Chen Y, Wang Y (2008) Doppler embolic signal detection using the adaptive wavelet packet basis and neurofuzzy classification. Pattern Recogn Lett 29(10):1589–1595
8. Chung G, Jeong J, Kwak H, Hwang S (2015) Associations between cerebral embolism and carotid intraplaque hemorrhage during protected carotid artery stenting. American Journal of Neuroradiology 37(4):686–691
9. Gencer M, Bilgin G, Aydin N (2013) Embolic doppler ultrasound signal detection via fractional fourier transform. In: Engineering in Medicine and Biology Society (EMBC), 35th Annual International Conference of the IEEE, pp 3050–3053
10. Girault JM, Zhao Z (2014) Synchronous detector as a new paradigm for automatic microembolus detection. International Journal of Biomedical Engineering and Technology 14(1):60–70
11. Huang YM, xin Du S (2005) Weighted support vector machine for classification with uneven training class sizes. In: Machine Learning and Cybernetics, 2005. Proceedings of 2005 International Conference on, vol 7, pp 4365–4369 Vol. 7
12. Karahoca A, Tunga MA (2015) A polynomial based algorithm for detection of embolism. Soft Computing 19(1):167–177

13. Karahoca A, Kucur T, Aydin N (2007) Data mining usage in emboli detection. In: Bio-inspired, Learning, and Intelligent Systems for Security, 2007. BLISS 2007. ECSIS Symposium on, pp 159–162
14. Krongold BS, Sayeed AM, Moehring M, Ritcey J, Spencer MP, Jones DL (1999) Time-scale detection of microemboli in flowing blood with doppler ultrasound. Biomedical Engineering, IEEE Transactions on 46(9):1081–1089
15. Marvasti S, Gillies D, Marvasti F, Markus HS (2004) Online automated detection of cerebral embolic signals using a wavelet-based system. Ultrasound in Medicine & Biology 30(5):647 – 653
16. Menigot S, Dreibine L, Meziati N, Girault J (2009) Automatic detection of microemboli by means of a synchronous linear prediction technique. In: Ultrasonics Symposium (IUS), 2009 IEEE International, pp 2371–2374
17. Mercer J (1909) Functions of positive and negative type, and their connection with the theory of integral equations. Philosophical Transactions of the Royal Society, London 209:415–446
18. Millioz F, Martin N (2010) Estimation of a white Gaussian noise in the short time Fourier transform based on the spectral kurtosis of the minimal statistics: Application to underwater noise. In: Acoustics Speech and Signal Processing (ICASSP), 2010 IEEE International Conference on, pp 5638–5641
19. Millioz F, Martin N (2011) Circularity of the stft and spectral kurtosis for time-frequency segmentation in Gaussian environment. IEEE Transactions on Signal Processing 59(2):515–524
20. Otsu N (1975) A threshold selection method from gray-level histograms. Automatica 11(285-296):23–27
21. Parzen E (1962) On estimation of a probability density function and mode. The Annals of Mathematical Statistics 33(3):pp. 1065–1076
22. Paschoal FM, de Almeida Lins Ronconi K, de Lima Oliveira M, Nogueira RdC, Paschoal EHA, Teixeira MJ, Figueiredo EG, Bor-Seng-Shu E (2015) Embolic signals during routine transcranial doppler ultrasonography in aneurysmal subarachnoid hemorrhage. BioMed research international 2015
23. Sarti A, Corsi C, Mazzini E, Lamberti C (2005) Maximum likelihood segmentation of ultrasound images with rayleigh distribution. Ultrasonics, Ferroelectrics, and Frequency Control, IEEE Transactions on 52(6):947–960
24. Sciolla B, Ceccato P, Dambry T, Guibert B, Delachartre P (2015) A comparison of non-parametric segmentation methods. In: GRETSI, Lyon, France, URL https://hal.archives-ouvertes.fr/hal-01307318
25. Serbes G, Aydin N (2014) Denoising performance of modified dual-tree complex wavelet transform for processing quadrature embolic doppler signals. Medical & biological engineering & computing 52(1):29–43
26. Smith J, Evans D, Fan L, Bell P, Naylor A (1996) Differentiation between emboli and artefacts using dual-gated transcranial doppler ultrasound. Ultrasound in Medicine & Biology 22(8):1031 – 1036
27. Sweeney KT, Ayaz H, Ward TE, Izzetoglu M, McLoone SF, Onaral B (2012) A methodology for validating artifact removal techniques for physiological signals. IEEE Transactions on Information Technology in Biomedicine 16(5):918–926
28. Wallace S, Døhlen G, Holmstrøm H, Lund C, Russell D (2015) Cerebral microemboli detection and differentiation during transcatheter closure of atrial septal defect in a paediatric population. Cardiology in the Young 25:237–244

Blaise Kévin Guépié received his Ph.D degree in statistical modeling from the Universit de Technologie de Troyes, in 2013. In 2014, He worked on prognostics and health management. He is currently post-doc and his research interests are time-frequency analysis, statistical signal processing, machine learning and edge detection at CREATIS, INSA Lyon, France.

Bruno Sciolla received his Ph.D in theoretical physics from the University of Paris-Sud, in 2012. Until 2014, he has conducted research in statistical physics of quantum systems, specifically the theory of ultracold atoms as a research fellow in the University of Geneva, Switzerland and in the University of Bonn, Germany. Since 2014 his research focuses on medical image processing, in particular image segmentation, motion estimation, and machine learning at CREATIS, INSA Lyon, France.

Fabien Millioz graduated from the École Normale Suprieure de Cachan, France and received the M.Sc. and Ph.D. degree in signal, image, and speech processing from the Institut National Poly-

technique of Grenoble, France, in 2005 and 2009, respectively. He was a postdoctoral research associate at the Institute for Digital Communications at the University of Edinburgh, UK, from 2009 to 2011. He is currently lecturer at the university of Lyon 1, associated to the Biomedical Imaging Research Lab Creatis. His research interests are time-frequency analysis, statistical signal processing, signal segmentation and deep neural networks.

Marilys Almar received the engineering diploma from INPG-ENSIEG Grenoble, France, in 2002. She is currently engineer in research and development at ATYS Medical company, Soucieu-en-Jarrest, France. Her research interests includes medical signal and image processing, blood flow analysis, HITS detection.

Philippe Delachartre received the Ph.D. degree from INSA Lyon, France, in 1994. He is currently a Professor with INSA Lyon. His research interests include motion estimation, segmentation, denoising, medical image analysis, ultrasound signal processing and ultrasound imaging.